*Acta Cryst.* (1997). B53, 750–761

# Thermal Expansion of Chemical Bonds

I. David Brown,* Antoni Dabkowski and Alison McCleary

*Brockhouse Institute for Materials Research, McMaster University, Hamilton, Ontario, Canada L8S 4M1. E-mail: idbrown@mcmaster.ca*

(*Received 23 December 1996; accepted 17 April 1997*)

## Abstract

Using the bond-valence model, a relationship is developed between the thermal expansion of a chemical bond, its amplitude of thermal vibration and its force constant. An empirical expression found between bond valence and the force constants derived from vibrational spectroscopy allows all of these quantities to be predicted from either the expected or the observed bond valence. The thermal expansion predicted by these relations is in excellent agreement with the average expansion observed around cations in inorganic solids, but individual bonds are found to expand more or less than this depending on strains and constraints within the structure. Comparison between the theoretical and observed amplitudes of thermal vibration gives a quantitative measure of correlation between the thermal motions of atoms that form the bond. The theory also shows how the parameters used in calculating bond valences from bond lengths should be corrected for temperature.

## 1. Introduction

The expansion that occurs when a crystal is heated is the net result of two effects: the expansion of bonds caused by the anharmonic potential between bonded atoms and the contraction (or expansion) in the distance between second nearest neighbours caused by the increased bending of the bond angles. Both effects are related to the increase in amplitude of the thermal motions of the atoms: vibrations along the direction of the bond causing bond expansion and vibrations perpendicular to the bonds causing bond bending.

In her classic study of thermal expansion Megaw (1939) analysed the problem of the thermal expansion of bonds in terms of Born potentials and proposed the empirical relation (1) between the coefficient of thermal expansion, $\alpha$, and the valence, $s$, of a bond

$$\alpha \propto s^{-2}. \quad (1)$$

Later, Hazen & Prewitt (1977) proposed a different empirical relation (2)

$$\alpha = 32.9(0.75 - s) \times 10^{-6}\ \mathrm{K}^{-1}. \quad (2)$$

Cameron, Sueno, Prewitt & Papike (1973) meanwhile demonstrated a negative linear correlation between the coefficient of thermal expansion and the force constant of a bond. In this paper we use the bond-valence model to derive theoretical relations between the force constant and thermal expansion of a bond, and the change in the amplitude of its thermal vibrations with temperature. These are each related to the bond valence through an empirical relation with the force constant. Although the theoretical relations derived here differ significantly from the empirical relationships previously proposed, they are found to agree well with observation.

According to the bond-valence model described by Brown (1992), every bond in a non-metallic inorganic crystal has a valence which obeys two rules: the sum of the bond valences around each atom is equal to the valence of the atom (valence-sum rule) and, subject to the valence-sum rule, the valence is distributed as equally as possible between the bonds (the equal-valence rule). These two rules, known as the network equations when expressed in mathematical form, can be used to predict the bond valences for any compound whose bond connectivity is known, a feature that we use in the analysis of individual structures below.

The usefulness of the bond-valence model lies in the empirical correlation found between bond valence, $s$, and bond length, $R$, given by

$$s = \exp((R_0 - R)/B), \quad (3)$$

where $R_0$ and $B$ are experimentally determined constants that depend only on the nature of the atoms that form the bond. Extensive tables of these constants determined at room temperature have been published by Brown & Altermatt (1985) and Brese & O'Keeffe (1991). Equation (3), which is plotted in Fig. 1, represents the repulsion between the atoms: the stronger a bond is made, the more difficult it is to shorten. It is therefore the bond-valence model's represention of the anharmonic part of the interatomic potential. Consequently, it should be possible to derive an expression for the thermal expansion of a bond starting with (3).

The application of the bond-valence model to thermal expansion makes use of the distortion theorem (Brown, 1992) which states that:

'If the bonds in the environment of an atom are changed in such a way as to lengthen some bonds and shorten others while keeping the sum of the bond valences constant, the average bond length will increase'.

The validity of this theorem can be seen from an examination of the graph of (3) shown in Fig. 1, where it is seen that the bond which is lengthened increases by much more than the decrease in the length of the bond that is shortened. Thus, the average bond length is increased providing the average bond valence is held constant, as required by the valence-sum rule.

This paper examines the hypothesis that the distortion theorem can be used to predict the thermal expansion of a bond in the following way. Suppose an atom is at the centre of a regular coordination sphere, *i.e.* all its bonds are the same length. As the temperature is raised, the atom will vibrate around its equilibrium position with an increasingly large amplitude. At any instant it will no longer be at the centre of its coordination sphere, but will be displaced a distance, $\delta\mathbf{R}$, from the centre. Thus, it will have some bonds that are longer and some shorter than the average, leading to the distortion theorem prediction that the average bond length will be increased. As the temperature is further increased, the amplitude of vibration will also increase and with it the average bond length. If one can predict how the amplitude of vibration changes with temperature, one can calculate the thermal expansion of the bond. This paper explores this hypothesis, using it in §2 to derive an expression for the thermal expansion of a bond and, in §3 and §4, to compare the values obtained from this expression with observations made on a number of crystals.

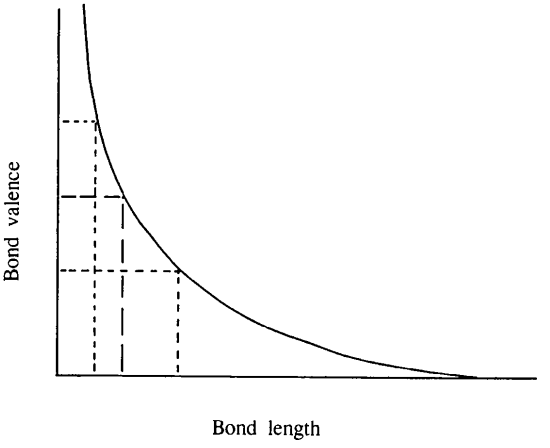


Fig. 1. Relationship between bond valence and bond length illustrating the distortion theorem. The long dashed lines indicate the valence and length in an undistorted coordination sphere; the short dashed lines are as in (*a*), but after distortion which keeps the average bond valence constant.

The increase in amplitude of vibration with temperature is primarily a harmonic effect – the anharmonic part of the interatomic potential produces only a second-order correction that can be neglected in the first approximation. However, the thermal expansion is an anharmonic effect. Equation (3) is used to calculate the instantaneous bond length at a given temperature. When the observed bond length is calculated by time-averaging over the instantaneous bond lengths, the first-order term in the Taylor expansion of the displacement vanishes, leaving only the second order or anharmonic term representing the thermal expansion. In the analysis below, therefore, it is satisfactory to calculate the amplitude of vibration of a bond in the harmonic approximation using the bond force constant, but the change in the average bond length requires the use of the anharmonic effects represented by (3).

## 2. Theory

### 2.1. *The relationship between dR/dT and dU/dT*

Assume that a cation is coordinated by $N$ bonds of length $R_i$ ($i$ = 1–$N$). First consider the change in length of one of these bonds. For simplicity we can then drop the index $i$. Assume also for the present that changing the temperature of the crystal does not alter the distribution of valence between the bonds so that the valence, $s$, of the bond under consideration remains constant as the temperature is raised. In this case (3) for the given bond can be written as

$$s = \exp((R_0 - R_e)/B), \tag{4}$$

where $R_e$ is the equilibrium length of the bond, *i.e.* the length of the bond when the atoms have no thermal motion and are stationary at their minimum energy positions.

At any given temperature the atoms are moving such that the instantaneous length of the bond, $R'$, is given by

$$R' = \langle R \rangle + \delta R,$$

where $\langle R \rangle$ is the time-averaged length of the bond (in general different from $R_e$ since the bond may expand on heating) and $\delta R$ will fluctuate with time, but will have an average value of zero.

From (3) $s'$, the instantaneous value of the bond valence, is then given by

$$\begin{aligned} s' &= \exp((R_0 - R')/B) \\ &= \exp((R_0 - (\langle R \rangle + \delta R))/B) \\ &= \exp((R_0 - \langle R \rangle)/B).\exp(-\delta R/B). \end{aligned}$$

Expanding the last term as a power series and ignoring the terms in high powers of the small quantity $\delta R$ gives

$$s' = \exp((R_0 - \langle R \rangle)/B)[1 - \delta R/B + \delta R^2/2B^2 + \ldots].$$

Averaging this equation over time and recognizing that $< s' >$, the time average of $s'$, is just $s$, since $s$ is assumed to be independent of temperature, yields

$$s = \exp((R_0 - < R >)/B)[1 + < \delta R^2 > /2B^2]$$

since the average of the term in the first power of $\delta R$ is zero.

Substituting the expression in (4) for $s$ and combining the two exponents gives

$$\exp((< R > - R_e)/B) = 1 + < \delta R^2 > /2B^2.$$

Since $\Delta R$ ($= < R > - R_e$) is the expansion in the bond resulting from thermal motion

$$\exp(\Delta R/B) = 1 + < \delta R^2 > /2B^2,$$

which, by expanding the left-hand side as a power series in the small quantity $\Delta R$ and dropping the higher order terms, gives

$$1 + \Delta R/B = 1 + < \delta R^2 > /2B^2$$

or

$$\Delta R = < \delta R^2 > /2B.$$

Since for most bonds $B$ can be taken as 0.37 Å (Brown & Altermatt, 1985), it follows that the increase in the bond length, relative to its length when the atoms are at rest, is related to the mean square deviation, $U \equiv < \delta R^2 >$, in the length of the bond by

$$\Delta R = 1.35U \text{ Å}. \tag{5}$$

Thus, the expansion of the bond is directly proportional to the mean square deviation of the bond from its mean length. In particular, recognizing that $R$ changes in the same way as $\Delta R$, and differentiating both sides with respect to temperature $T$, gives

$$dR/dT = d\Delta R/dT = 1.35(dU/dT). \tag{6}$$

### 2.2. *Determination of dU/dT*

The value of $U$ depends on the thermal motions of both the central atom and its ligand. It can be determined only if we know the amplitudes of motion of both atoms along the direction of the bond and how their relative motions correlate. The amplitude can be measured by X-ray diffraction, but the correlation is not so readily determined. However, we can identify two limiting cases, the first when the two atoms are connected by a rigid bond and therefore always move in-phase and the second when their motions are uncorrelated.

In the rigid-bond limit the atom and its ligand are rigidly connected and so have identical motions along the bond direction. $\delta R$, hence $U$, is therefore identically zero, regardless of the degree of thermal motion, and (5) predicts that the bond will show no thermal expansion. Hirschfeld (1976) has shown that such rigid bonds have atomic displacement parameters with identical components along the vector that joins them. Rigid bonds are typically found in strongly bonded complexes such as $SO_4^{2-}$, $PO_4^{3-}$ and $SiO_4^{4-}$.

Uncorrelated motion is most likely to be found when the bonds are weak, for example, when the cation is a large alkali metal. In this case the mean square deviation of the bond length is given by the sum of the components of the atomic displacement parameters, **U**, of the two atoms along the bond direction (Busing & Levy, 1964), so that

$$< \delta R^2 > = (\mathbf{U}_{\text{cation}} + \mathbf{U}_{\text{anion}}).\mathbf{r} \equiv U(+),$$

where **r** is a unit vector in the direction of the bond. Therefore, from (5) the thermal expansion of weak bonds is predicted to be

$$\Delta R = 1.35U(+) \text{ Å} \tag{7}$$

and (6) can be written as

$$dR/dT = c.dU(+)/dT,$$

where for rigid bonds $c = 0$ and for bonds whose terminal atoms have uncorrelated motions $c = 1.35$. For all other bonds $c$ will lie between these extremes. This result is in good agreement with the value of $c$ of $\sim$0.7 derived from Fig. 16 of Cameron *et al.* (1973), which shows the correlation between the average coefficient of thermal expansion of a bond and the average thermal increase in the isotropic displacement parameters for different cations.

The problem of the unknown correlation between the motions of the terminal atoms can be avoided if it is possible to make a direct determination of $dU/dT$. Even though $U$ cannot be measured experimentally, it can be calculated by noting that in the classical harmonic approximation, which should be adequate for calculating $U$ above room temperature, the energy in the bond is $GA^2/2$, where $G$ is the force constant of the bond and $A$ is its amplitude of vibration. Boltzmann's equation then gives

$$U = [\int A^2 \exp(-GA^2/2kT)dA]/[\int \exp(-GA^2/2kT)dA] = kT/G, \tag{8}$$

where the integration is taken over all values of $A$. The derivative has the simple form

$$dU/dT = k/G. \tag{9}$$

Force constants can be determined from the analysis of vibrational spectra, but such analyses have not been performed for most of the crystal used in this study, so it is necessary to look for a relation that will permit force constants to be predicted from structural information. A selection of force constants taken from the literature is plotted in Fig. 2 as a function of the bond valence $s$. The scatter among these values can be attributed to the weakness of the assumptions implicit in the use of the Urey–Bradley force field, as well as to experimental error and the neglect of determinative factors other than bond valence, but in spite of the scatter, a clear trend is observed and a reasonable description is given by (10), which is designed to give a quadratic fit at $s = 0$ and a linear fit for $s > 1$ v.u.

$$G = as - b(1 - \exp(-as/b)). \quad (10)$$

The constants $a$ and $b$, which correspond to the solid line in Fig. 2, are $450\ \mathrm{N\,m^{-1}}$ (v.u.)$^{-1}$ and $140\ \mathrm{N\,m^{-1}}$, respectively. However, bonds to atoms that lie low in the periodic table tend to lie below this line, while those high in the table tend to lie above, introducing a small systematic error in the estimate of $G$ given by (10). To make explicit the extent of the uncertainty introduced by this error, two limiting broken lines are also shown, the upper having $a = 505\ \mathrm{N\,m^{-1}}$ (v.u.)$^{-1}$ and $b = 100\ \mathrm{N\,m^{-1}}$, and the lower having $a = 405\ \mathrm{N\,m^{-1}}$ (v.u.)$^{-1}$ and $b = 200\ \mathrm{N\,m^{-1}}$.

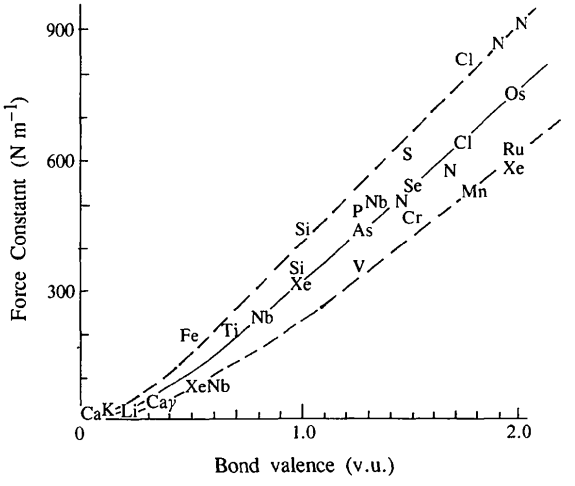


Fig. 2. Correlation between force constant and bond valence from spectroscopic measurements. The lines represent equation (10). Force constants taken from Amos & Flewett (1974): $Ti(NO_3)_4$; Armbruster (1976): $YXO_4$; Deverajan & Shurvell (1977): $Li_2SiO_3$; Galanov & Brodskii (1969): $KClO_4$; Husson, Repelin, Dao & Brusset (1977): $CaNb_2O_6$; Jones, Swanson & Kubas (1974): $Cs_2LiFe(CN)_6$; Müller & Krebs (1967): $XO_4$ species; Plihal & Schaak (1970): $CaCO_3$; Willett, LaBonville & Ferraro (1975): $XeO_2F_2$. The points are labelled by the cation, the anions are first-row elements, mostly oxygen.

As discussed in §4.1, the validity of (9) can be tested by comparing the values of $dU/dT$ calculated using (9) and (10) with the values of $dU(+)/dT$ obtained from diffraction studies (Fig. 3) since

$$0 \le dU/dT = k/G \le dU(+)/dT. \quad (11)$$

A factor $f$, which measures the degree of correlation between the motions of the terminal atoms, is given by

$$f = 1 - (dU/dT)/(dU(+)/dT). \quad (12)$$

A direct prediction of the thermal expansion of a bond in terms of its force constant, $G$, is obtained by combining (6) and (9)

$$dR/dT = 1.35k/G. \quad (13)$$

Using (10) to calculate $G$ it is possible to use (13) to calculate $dR/dT$ as a function of bond valence. The result is shown by the solid lines in Figs. 4 and 5. The broken lines show the values of $dR/dT$ that correspond to the broken lines of Fig. 2.

It should be pointed out that (10) and (13), which are used to give $dR/dT$ as a function of bond valence, are dependent only on three fitted parameters: $B$ in (3) is obtained by fitting bond lengths to bond valences and is known to have a value close to 0.37 Å for most if not all bonds (Brown & Altermatt, 1985), and $a$ and $b$ in (10) are obtained by fitting force constants to bond valences as shown in Fig. 2. None of the parameters have been chosen to fit the temperature dependence of any bond property. The extent to which the theory describes the observations is the extent to which the underlying model can be considered valid.

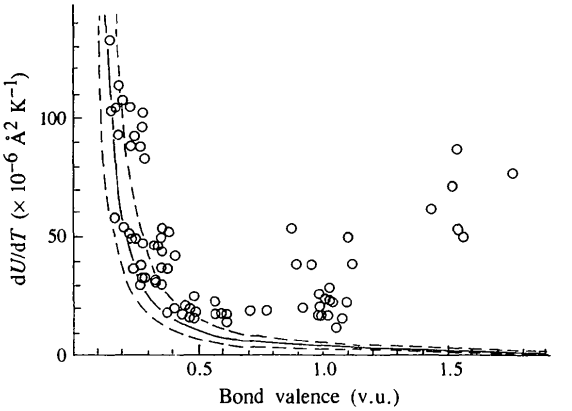


Fig. 3. $dU/dT$ *versus* bond valence. The circles refer to the observed values of $dU(+)/dT$ given in Table 1. The solid line represents equation (9), the broken lines represent the limits shown in Fig. 2.

### 2.3. *The variation of $R_0$ with temperature*

A by-product of this analysis is the determination of how the bond-valence parameter $R_0$ of (3) varies with temperature. The tabulated values (Brown & Altermatt, 1985; Brese & O'Keeffe, 1991) have generally been determined at room temperature and are clearly inappropriate for use when analysing structures determined at other temperatures. The bond-valence parameters can, however, be simply corrected for temperature by noting that at higher temperature, when the bond has expanded by $\Delta R$, (3) can be written as

$$s = \exp(((R_0 + \Delta R) - (R + \Delta R))/B).$$

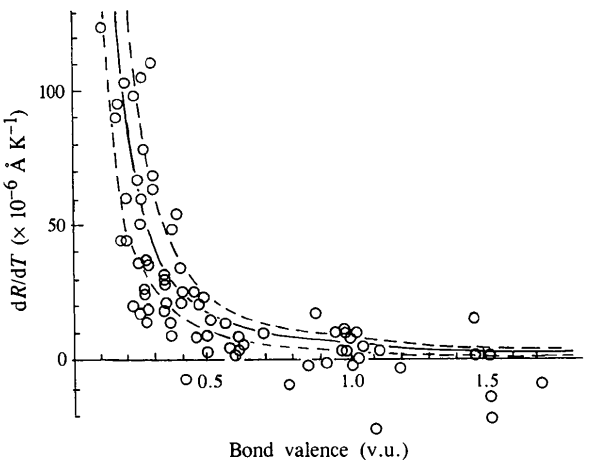


Fig. 4. $dR/dT$ *versus* bond valence for individual bonds. The circles refer to the observed values given in Table 1. The solid line shows the predictions obtained from (13) and the broken lines represent the limits shown in Fig. 2.

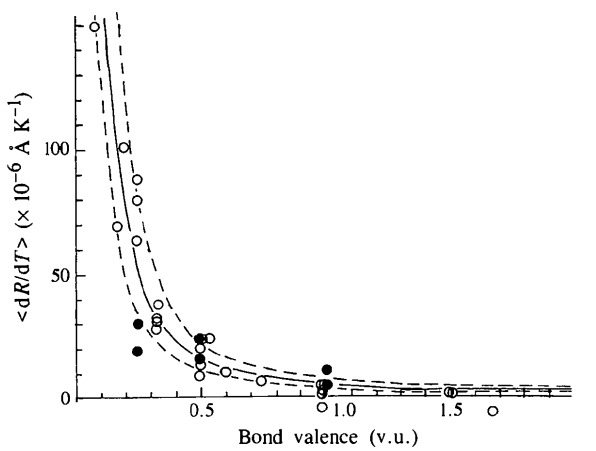


Fig. 5. $\langle dR/dT \rangle$ averaged around each cation *versus* bond valence. The circles refer to the averages of the observed values given in Table 1. The filled circles refer to the garnets (*f* and *g*). The lines are the same as those shown in Fig. 4.

Thus, $R_0^T$, the value of $R_0$ to be used at temperature $T$ above room temperature, is given by

$$R_0^T = R_0 + \Delta R = R_0 + (dR/dT)\Delta T. \qquad (14)$$

Reasonable values of $dR/dT$ as a function of $s$ can be found from the solid line shown in Fig. 5.

### 2.4. *The influence of strains and constraints*

The above analysis assumes that changes in temperature do not change the distribution of valence between the bonds. However, this ideal is not always achieved in practice, particularly in strained or constrained structures. The requirements of translational symmetry impose constraints that sometimes make it impossible for the bonds to adopt the chemically ideal lengths predicted by the network equations described in §1. Consequently, bonds in inorganic solids are sometimes strained, as identified by differences between the predicted and observed bond valences (see Table 1 for examples). Bonds in which the observed valences are lower than predicted are stretched, whilst those in which the observed valences are higher are compressed.

Such strains may influence the degree to which a given bond is able to expand with temperature. For example, one might expect the thermal expansion of a stretched bond to be larger than that of a bond that is compressed, leading to a redistribution of the bond valence. Thermal expansion will thus exaggerate any strains in the environment of an atom.

Another source of valence redistribution is found in structures that are constrained by having two or more different chains of bonds running in parallel through the crystal. Both chains must expand at the same rate which will be determined by the expansion of the more strongly bonded chain. The weaker bonds are thus constrained to expand at a lower rate than theory would predict and, to conserve the valence sum at each atom, valence is transferred from the bonds perpendicular to the chain to those parallel to the chain as the temperature is increased. Thus, the bonds perpendicular to the chains will expand more than expected.

## 3. Experimental

In order to test the predictions of the model, the Inorganic Crystal Structure Database (ICSD; Bergerhoff, Sievers, Hundt & Brown, 1983) was searched for compounds whose structures have been determined at various temperatures between room temperature and 1000 K, without displaying any phase or ordering transitions. The compounds retrieved were chosen to have relatively simple structures with no hydrogen bonds, to be well determined and to have been refined with anisotropic atomic displacement parameters. A total of 12 compounds, listed in Table 1, were chosen for analysis.

Table 1. *Theoretical and observed bond valences, thermal expansion dR/dT, dU(+)/dT and f for bonds in various structures*

Uncertainties obtained from regressions are given at the 90% confidence limit. The header for each compound gives the formula, name, ICSD collection number, space group, temperature range studied and the number of determinations used.

| | Bond valence | | $dR/dT$ ($\times10^{-6}$ Å K$^{-1}$) | | $dU/dT$ | $dU(+)/dT$ ($\times10^{-6}$ Å$^2$ K$^{-1}$) | Correlation factor |
|---|---|---|---|---|---|---|---|
| Bond | Theor. | Obs. | Theor. | Obs. | Theor. | Obs | $f$ |
| (*a*) $CuAlO_2$ | Delafossite (ICSD 32630-5) | | | *R*$\bar{3}$*m* | | 295-1200 K | 6 |
| Cu—O ×2 | 0.50 | 0.49 | 16 | 9 (3) | 12 | 21 (2) | 0.43 |
| Al—O ×6 | 0.50 | 0.46 | 16 | 20 (2) | 12 | 22 (3) | 0.45 |
| (*b*) BaClF | (ICSD 201514-9) | | | *P*4/*nmm* | | 297-883 K | 6 |
| Ba—F ×4 | 0.25 | 0.29 | 53 | 64 (4) | 37 | 103 (10) | 0.64 |
| Ba—Cl1 | 0.20 | 0.22 | 78 | 99 (6) | 53 | 108 (5) | 0.51 |
| Ba—Cl2 ×4 | 0.20 | 0.18 | 78 | 103 (7) | 53 | 106 (10) | 0.50 |
| (*c*) $LiIO_3$ | (ICSD 46025-27, 35474-6) | | | $P6_3$ | | 299-460 K | 3 |
| Li—O ×3 | 0.17 | 0.19 | 103 | 44 (7) | 78 | 116 (11) | 0.33 |
| Li—O′ ×3 | 0.17 | 0.16 | 103 | 95 (49) | 78 | 105 (7) | 0.26 |
| I—O ×3 | 1.67 | 1.72 | 3 | −8 (52) | 2 | 75 (11) | 0.97 |
| (*d*) $Ni_2SiO_4$ | (ICSD 100642-5) | | | *Pbnm* | | 298-1173 K | 4 |
| Ni1—O1 ×2 | 0.33 | 0.34 | 32 | 30 (10) | 23 | 32 (3) | 0.28 |
| Ni1—O2 ×2 | 0.33 | 0.33 | 32 | 31 (19) | 23 | 33 (9) | 0.30 |
| Ni1—O3 ×2 | 0.33 | 0.29 | 32 | 35 (11) | 23 | 33 (12) | 0.30 |
| Ni2—O1 | 0.33 | 0.28 | 32 | 37 (23) | 23 | 34 (15) | 0.32 |
| Ni2—O2 | 0.33 | 0.36 | 32 | 14 (10) | 23 | 32 (17) | 0.28 |
| Ni2—O3 ×2 | 0.33 | 0.24 | 32 | 36 (12) | 23 | 38 (10) | 0.39 |
| Ni2—O3′ ×2 | 0.33 | 0.34 | 32 | 21 (9) | 23 | 37 (15) | 0.38 |
| Si—O1 | 1.00 | 1.06 | 6 | 6 (8) | 4 | 13 (8) | 0.69 |
| Si—O2 | 1.00 | 0.92 | 6 | −0 (13) | 4 | 21 (8) | 0.81 |
| Si—O3 ×2 | 1.00 | 1.03 | 6 | −1 (10) | 4 | 24 (8) | 0.83 |
| (*e*) $Fe_2SiO_4$ | (ICSD 10116-8) | | | *Pbnm* | | 573-1173 K | 4 |
| Fe1—O1 ×2 | 0.33 | 0.34 | 32 | 29 (5) | 23 | 49 (7) | 0.53 |
| Fe1—O2 ×2 | 0.33 | 0.34 | 32 | 18 (7) | 23 | 49 (5) | 0.53 |
| Fe1—O3 ×2 | 0.33 | 0.27 | 32 | 27 (9) | 23 | 51 (4) | 0.55 |
| Fe2—O1 | 0.33 | 0.26 | 32 | 24 (2) | 23 | 51 (2) | 0.55 |
| Fe2—O2 | 0.33 | 0.37 | 32 | 14 (6) | 23 | 39 (6) | 0.41 |
| Fe2—O3 ×2 | 0.33 | 0.21 | 32 | 20 (8) | 23 | 56 (4) | 0.57 |
| Fe2—O3′ ×2 | 0.33 | 0.38 | 32 | 54 (16) | 23 | 56 (11) | 0.57 |
| Si—O1 | 1.00 | 1.03 | 6 | 12 (14) | 4 | 28 (10) | 0.86 |
| Si—O2 | 1.00 | 0.95 | 6 | 12 (12) | 4 | 38 (4) | 0.89 |
| Si—O3 ×2 | 1.00 | 1.10 | 6 | −27 (13) | 4 | 49 (12) | 0.92 |
| (*f*) $Mg_3Al_2(SiO_4)_3$ | Pyrope | | (ICSD 24940-3) | | *Ia*3*d* | 298-1023 K | 4 |
| Mg—O ×4 | 0.25 | 0.26 | 53 | 16 (11) | 37 | 32 (21) | −0.16 |
| Mg—O′ ×4 | 0.25 | 0.17 | 53 | 44 (3) | 37 | 61 (5) | 0.39 |
| Al—O ×6 | 0.50 | 0.49 | 16 | 14 (3) | 12 | 25 (8) | 0.52 |
| Si—O ×4 | 1.00 | 1.01 | 6 | 1 (5) | 4 | 20 (12) | 0.80 |
| (*g*) $Ca_3Al_2(SiO_4)_3$ | Grossular (ICSD 24944-6) | | | *Ia*3*d* | | 298-948 K | 3 |
| Ca—O ×4 | 0.25 | 0.39 | 53 | 22 (11) | 37 | 20 (16) | −0.85 |
| Ca—O′ ×4 | 0.25 | 0.24 | 53 | 18 (4) | 37 | 39 (6) | 0.05 |
| Al—O ×6 | 0.50 | 0.44 | 16 | 25 (1) | 12 | 22 (4) | 0.45 |
| Si—O ×4 | 1.00 | 0.98 | 6 | 12 (7) | 4 | 26 (8) | 0.85 |
| (*h*) $BaSO_4$ | (ICSD 33730-4) | | | *Pnma* | | 298-1158 K | 5 |
| Ba—O1 | 0.40 | 0.28 | 23 | 110 (20) | 17 | 89 (23) | 0.81 |
| Ba—O2 | 0.40 | 0.26 | 23 | 78 (9) | 17 | 94 (27) | 0.82 |
| Ba—O3 ×2 | 0.20 | 0.25 | 78 | 106 (20) | 53 | 91 (12) | 0.42 |
| Ba—O3′ ×2 | 0.20 | 0.19 | 78 | 60 (28) | 53 | 94 (12) | 0.44 |
| Ba—O3″ ×2 | 0.20 | 0.25 | 78 | 60 (30) | 53 | 106 (16) | 0.50 |
| S—O1 | 1.60 | 1.54 | 3 | −22 (33) | 2 | 85 (33) | 0.98 |
| S—O2 | 1.60 | 1.53 | 3 | −14 (24) | 2 | 70 (28) | 0.97 |
| S—O3 ×2 | 1.40 | 1.46 | 3 | 16 (24) | 3 | 61 (26) | 0.95 |
| (*i*) $MgGeO_3$ | Pyroxene (ICSD 201660-201663) | | | *C*2/*c* | | 293-893 K | 4 |
| Mg1—O1 ×2 | 0.30 | 0.36 | 40 | 10 (16) | 28 | 46 (6) | 0.39 |
| Mg1—O1′ ×2 | 0.30 | 0.30 | 40 | 49 (8) | 28 | 52 (20) | 0.46 |
| Mg1—O2 ×2 | 0.40 | 0.39 | 23 | 34 (5) | 17 | 55 (20) | 0.69 |
| Mg2—O1 ×2 | 0.35 | 0.23 | 23 | 51 (16) | 22 | 51 (17) | 0.57 |
| Mg2—O2 ×2 | 0.45 | 0.41 | 19 | −6 (9) | 14 | 44 (17) | 0.68 |

Table 1 (*cont.*)

| Bond | Bond valence Theor. | Obs. | $dR/dT$ ($\times10^{-6}$ Å K$^{-1}$) Theor. | Obs. | $dU/dT$ Theor. | $dU(+)/dT$ ($\times10^{-6}$ Å$^2$ K$^{-1}$) Obs | Correlation factor $f$ |
|---|---|---|---|---|---|---|---|
| Mg2—O3 ×2 | 0.20 | 0.24 | 78 | 68 (31) | 53 | 54 (18) | 0.02 |
| Ge—O1 | 1.05 | 1.03 | 6 | 0 (8) | 4 | 24 (8) | 0.83 |
| Ge—O2 | 1.15 | 1.12 | 5 | 4 (6) | 4 | 33 (9) | 0.88 |
| Ge—O3 | 0.90 | 0.88 | 7 | 18 (4) | 5 | 38 (11) | 0.87 |
| Ge—O3 | 0.90 | 0.86 | 7 | −1 (26) | 5 | 54 (27) | 0.91 |
| (*j*) $KLiSO_4$ | (ICSD 36470-36472) | | | $P6_3$ | | 293–568 K | 3 |
| Li—O1 | 0.23 | 0.30 | 62 | 224 (349) | 42 | 85 (14) | 0.51 |
| Li—O2 ×3 | 0.26 | 0.29 | 51 | 44 (84) | 30 | 98 (6) | 0.69 |
| K—O1 ×3 | 0.10 | 0.10 | 306 | 125 (21) | ~210 | 214 (1) | ~0 |
| K—O2 ×3 | 0.12 | 0.15 | 204 | 91 (4) | ~150 | 135 (2) | ~0 |
| K—O2′ ×3 | 0.12 | 0.10 | 204 | 240 (82) | ~150 | 198 (22) | ~0 |
| S—O1 | 1.48 | 1.54 | 3 | −238 (20) | 3 | 54 (6) | 0.94 |
| S—O2 ×3 | 1.51 | 1.57 | 3 | −63 (18) | 3 | 52 (7) | 0.94 |
| (*k*) $Al_2SiO_5$ | Andalusite | (ICSD 100395-7) | | *Pnnm* | | 300–1273 K | 5 |
| Al1—O1 ×2 | 0.47 | 0.48 | 17 | 2 (1) | 13 | 19 (1) | 0.32 |
| Al1—O3 ×2 | 0.61 | 0.57 | 12 | 4 (1) | 8 | 19 (1) | 0.58 |
| Al1—O4 ×2 | 0.42 | 0.28 | 22 | 69 (2) | 16 | 48 (2) | 0.67 |
| Al2—O2 | 0.53 | 0.55 | 14 | 14 (3) | 11 | 21 (2) | 0.48 |
| Al2—O2′ | 0.53 | 0.47 | 14 | 23 (6) | 11 | 20 (1) | 0.45 |
| Al2—O3 | 0.78 | 0.59 | 9 | 9 (2) | 6 | 20 (1) | 0.70 |
| Al2—O4 ×2 | 0.58 | 0.59 | 13 | 4 (1) | 10 | 20 (1) | 0.50 |
| Si—O1 | 1.06 | 0.98 | 5 | 3 (3) | 4 | 21 (1) | 0.81 |
| Si—O2 | 0.94 | 1.06 | 6 | 1 (3) | 5 | 17 (2) | 0.71 |
| Si—O4 ×2 | 1.00 | 1.03 | 6 | −1 (2) | 4 | 18 (1) | 0.78 |
| (*l*) $Al_2SiO_5$ | Sillimanite | (ICSD 100450-4) | | *Pbnm* | | 300–1273 K | 5 |
| Al1—O1 ×2 | 0.50 | 0.45 | 16 | 9 (3) | 12 | 20 (2) | 0.40 |
| Al1—O2 ×2 | 0.59 | 0.57 | 12 | 4 (1) | 10 | 24 (5) | 0.58 |
| Al1—O4 ×2 | 0.42 | 0.40 | 22 | 25 (4) | 16 | 23 (1) | 0.30 |
| Al2—O2 | 0.83 | 0.70 | 8 | 10 (2) | 5 | 20 (2) | 0.75 |
| Al2—O3 | 0.86 | 0.78 | 7 | −9 (2) | 5 | 22 (2) | 0.77 |
| Al2—O4 ×2 | 0.66 | 0.62 | 11 | 6 (2) | 7 | 19 (1) | 0.63 |
| Si—O1 | 1.01 | 1.00 | 6 | 6 (4) | 4 | 18 (1) | 0.78 |
| Si—O3 | 1.14 | 1.20 | 5 | −2 (3) | 4 | 22 (2) | 0.82 |
| Si—O4 ×2 | 0.93 | 0.99 | 7 | 5 (4) | 5 | 17 (1) | 0.71 |

A number of errors were found in the database, many of them traceable to errors or ambiguities in the original literature. The atomic displacement parameters were checked particularly carefully. Errors in the positional coordinates, which can be readily detected when bond lengths are calculated, are by no means unknown in the literature; how much more should we expect to find errors in the displacement parameters, which cannot be so easily checked? Displacement parameters are also strongly affected by systematic errors such as absorption, but since these effects tend to be the same for all measurements made on the same crystal, this should not affect the variation of atomic displacement parameters with temperature. A second source of error lies in the confusion which arises from the way displacement parameters are reported, since there are several different conventions in use. They can be reported in the form of $B$, $\beta$ or $U$, each with a different definition. Further, there are two different definitions of $\beta$ depending on whether the factor of 2 in the cross terms is included explicitly or is incorporated in the value of $\beta$ itself and authors do not always state which convention they have adopted. Fortunately, in the cases studied the results were not significantly affected by this ambiguity. A third type of error can occur if the crystallographic setting is transformed between refinement and publication, since the transformation can easily be applied incorrectly to the displacement parameters. This danger is augmented if the author does not give explicitly the atomic positional coordinates fixed by symmetry for atoms on special positions. An inexcusable error, but one that is known to occur, arises because different refinement programs list the elements of the atomic **U** matrices in a different order, leading to the possibility of careless transcription. Therefore, extreme caution is needed in interpreting the reported displacement parameters. While several correctable errors were found in the atomic displacement parameters reported in the ICSD, there may well be others that we did not catch. Some compounds were excluded from the study because of doubts about the correctness of these parameters.

For each bond at each of the reported temperatures the values of $R$, $(\mathbf{U}_{\text{cation}} + \mathbf{U}_{\text{anion}}).\mathbf{r} \equiv U(+)$ and $(\mathbf{U}_{\text{cation}} - \mathbf{U}_{\text{anion}}).\mathbf{r}$ were calculated, the latter being used to check

the atomic displacement parameters. Its value should be close to zero, particularly for rigid bonds (Busing & Levy, 1964). Large and variable values indicate possible problems in the reported values of U. The results of a regression analysis of $R$ and $U(+)$ on $T$ are reported as $dR/dT$ and $dU(+)/dT$ in Table 1, the number in parentheses in each case representing the 90% confidence limit generated by the regression analysis.

## 4. Results

The results of this study are summarized in Table 1. For each of the 80 bonds in the 12 crystals studied, the theoretical and observed bond valences are given, the theoretical values being calculated using the network equations mentioned in §1 and described in more detail by Brown (1992). Where the bonds are strained, these two values are different. A stretched bond is indicated by an observed valence smaller than theory and a compressed bond by an observed valence greater than theory. Then follow the theoretical values of $dR/dT$ calculated by substituting the theoretical bond valences into (10) to find $G$, which is substituted into (13) to obtain $dR/dT$. The next columns give the observed values of $dR/dT$, the theoretical value of $dU/dT$ [from (10) and (9)] and the observed value of $dU(+)/dT$ followed by the correlation factor $f$, given by (12). For each compound the information given in the header is a reference letter, the formula, the ICSD collection numbers, the space group, the temperature range examined and the number of temperatures at which structures were determined. Further details of individual structures are given in §4.3.

### 4.1. *Comparison of $dU/dT$ with $dU(+)/dT$*

Fig. 3 shows the observed values of $dU(+)/dT$, indicated by circles, and $dU/dT$, calculated using (9) and (10) and indicated by the solid line, plotted against bond valence. The broken lines correspond to the values of $dU/dT$ that would be obtained using the broken lines of Fig. 2. As expected, the points for $dU(+)/dT$ lie on or above the line [see (11)]. The difference is largest for the strong bonds. These are the bonds that are expected to be rigid, for which the assumption of uncorrelated motion is not valid.

The correlation between the motion of the two atoms defining a bond is given by the correlation factor $f$ defined in (12) and plotted in Fig. 6. A value of zero represents no correlation and 1.0 a rigid bond. The solid line shown in this figure has the equation

$$f = 1 - \exp(-s/0.5). \qquad (15)$$

Much of the scatter in this plot can be attributed to the scatter observed in Fig. 2. In particular, the error introduced by ignoring the size of the atoms in (10) results in bonds formed by atoms low in the periodic table appearing to have too large a correlation (*e.g.* $b$ and $h$) and those formed by atoms high in the periodic table to have too small a correlation (*e.g.* $k$ and $l$). The solid line therefore represents a better estimate of the correlation than the individual observations.

The agreement between observation and the expectations of the theory indicate that, in spite of the assumptions made in deriving (10) and (9), $dU/dT$ gives a reliable prediction of the increase in the amplitude of vibration of bonds with temperature. This means that these equations can be used with confidence in predicting the thermal expansion of the bonds.

### 4.2. *Comparison of the theoretical and observed values of $dR/dT$*

The solid line in Fig. 4 shows the theoretical values of $dR/dT$, calculated using (10) and (13), as a function of bond valence. The circles represent the values observed for individual bonds. There is general agreement between theory and observation, but a significant number of observations lie outside the limits of uncertainty indicated by the broken lines calculated from the broken lines of Fig. 2. The negative expansions shown for some of the stronger bonds are generally smaller than the experimental uncertainty, but the librational motions of strongly bonded groups such as $SO_4$ and $IO_3$ are expected to give rise to an apparent thermal contraction of the bonds (Busing & Levy, 1964; Schomaker & Trueblood, 1968). No correction was made for this effect.

Better agreement can be obtained if the values of $dR/dT$ are averaged over all the bonds around a given cation, as shown in Fig. 5. With the exception of the garnets (indicated by filled circles), most of the points in this figure now lie between the broken lines, suggesting that the scatter seen in Fig. 4 results from the redistribution of valence between the bonds. Deviations from the predicted pattern are discussed for each structure in the next section.

The solid line shown in Figs. 4 and 5 differs significantly from earlier proposed correlations. In the these studies the expansion was expressed in terms of the

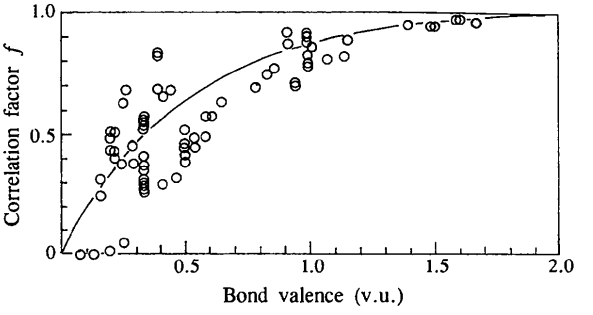


Fig. 6. Correlation factor $f$ in (12) *versus* bond valence for individual bonds. The line represents (15).

coefficient of thermal expansion, $\alpha$, which is related to $dR/dT$ by

$$\alpha = (dR/dT)/R. \quad (16)$$

Since $R$ is relatively constant, varying between *ca* 1.5 and 2.5 Å, depending on the atoms that form the bond, an approximate comparison can be made by assuming a value of 2 Å. Megaw's (1939) expression (1) approximates the line shown in Fig. 5 and, with a suitable choice of proportionality constant, can be made to lie between the broken lines, but it overestimates $\alpha$ for the weak bonds and underestimates it for the strong bonds. Hazen & Prewitt's (1977) relation (2), on the other hand, corresponds to an almost straight line that is tangent to the solid curve of Fig. 5 at 0.45 v.u. Their equation agrees reasonably well with the present theory over the range 0.3–0.5 v.u., but greatly underestimates the expansion outside this range.

### 4.3. *Discussion of individual structures*

4.3.1. *$CuAlO_2$ delafossite (a).* The crystals of $CuAlO_2$ were examined between 295 and 1200 K by Ishiguro, Ishizawa, Mizutani & Kato (1982), who also analysed the changes in structure with temperature.

The delafossite structure contains hexagonal planes of edge-sharing $AlO_6$ octahedra linked by linear O—Cu—O bridges lying along the rhombohedral threefold axis. The short 2.858 Å Cu—Cu and Al—Al spacing perpendicular to the rhombohedral axis is determined by the size of the edge-sharing $AlO_6$ octahedra and results in strong cation–cation repulsions. Consequently, the $AlO_2$ layers are stretched in the basal plane, with the octahedra flattened perpendicular to the layer and the Al—O bonds stretched from 1.876 to 1.911 Å (the observed bond valence of 0.46 v.u. can be compared with the expected value of 0.50 v.u.).

Since the Al—O bonds are stretched, the observed value of $dR/dT$ for the Al—O bonds is larger than that predicted by the theory (Table 1). Redistribution of valence around O results in the Cu—O bonds having a lower than predicted expansion.

4.3.2. *BaClF (b).* This compound was examined over the range 297–883 K by Kodama, Tanaka, Utsunomiya, Hoshino, Marumo, Ishizawa & Kato (1984). Its tetragonal structure consists of layers containing two F atoms alternating with two BaCl layers, each Ba atom forming four bonds to an adjacent F layer, four bonds to Cl atoms in its own BaCl layer and one bond to Cl in the adjacent BaCl layer. All four Ba—F distances are equal, but the interlayer and intralayer Ba—Cl distances are crystallographically distinct.

As Ba is a heavy atom, the force constants tend to be overestimated by (10), giving a theoretical value for $dR/dT$ which is too low. $dU/dT$ is correspondingly underestimated and the correlation coefficient $f$ overestimated, leading to points that lie above the line in Fig. 6. Using the lower broken curve in Fig. 2, for example, gives improved theoretical values for $dR/dT$ of 85 and $123 \times 10^{-6}$ Å K$^{-1}$.

4.3.3. *$LiIO_3$ (c).* The structure of $LiIO_3$ has been reported by Coquet, Crettez, Pannetier, Bouillot & Damien (1983) over the range 373–525 K using neutron diffraction and by Svensson, Albertson, Liminga, Kvick & Abrahams (1983) over the range 299–460 K using X-ray diffraction. The results of the study by Coquet *et al.* (1983) showed less consistency than those of Svensson *et al.* (1983) and were not used.

The structure contains a pyramidal $IO_3$ ion, which is a tetrahedral ion with one ligand position occupied by a lone electron pair. The ions are arranged so as to provide columns of face-sharing octahedral sites that are occupied by Li. Given that the uncertainty in the observed position of the Li atom is of the same order as the thermal expansion, agreement between the theoretical and observed values of $dR/dT$ and $dU/dT$ is satisfactory.

4.3.4. *$Fe_2SiO_4$ (d) and $Ni_2SiO_4$ (e).* The structure of Ni olivine has been determined by Lager & Meagher (1978) between 298 and 1174 K and that of the Fe olivine fayalite by Smyth (1975) between 293 and 1173 K.

The two compounds are isostructural. All four Si—O bonds are chemically equivalent, *i.e.* have the same connectivity, and therefore have a predicted valence of 1.00 v.u. The *M*—O bonds are likewise chemically equivalent with a predicted valence of 0.33 v.u. Deviations from these values are the result of strains. The environment of *M*1 is close to ideal in both compounds, but that around *M*2 is distorted because the *M*2 atom sits in a cavity that is too large, indicated by the valence sum around *M*2 being only 1.80 rather than 2.00 v.u. Consequently, *M*2 is displaced from the centre of the cavity, away from the edge shared with the $SiO_4$ tetrahedron, giving three weak and three strong bonds. The resulting strengthening of the *M*2—O2 bond and weakening of the *M*2—O1 bond is responsible for the distortions observed in the $SiO_4$ tetrahedron.

The agreement between theory and observation is satisfactory for $Ni_2SO_4$. The variation in the thermal expansion of the bonds formed by Ni2 follows the expectation that the stronger bonds will expand less than the weaker ones. A similar pattern is seen for $Fe_2SiO_4$, except that $dU(+)/dT$ is systematically larger and the bonds formed by O3 are anomalous. Too much significance should not be read into these anomalies, since they would disappear if O3 were shifted by three times the standard uncertainty in its position.

4.3.5. *$Mg_3Al_2(SiO_4)_3$ (f) and $Ca_3Al_2(SiO_4)_3$ (g).* The structure of the aluminosilicate garnets, pyrope (Mg) and grossular (Ca), have been studied by Meagher (1975) between room temperature and 1000 K. He gives references to previous systematic studies as well as a summary of the differences in the thermal behaviour of

a range of Al—Si garnets, of which these two represent the end members, Mg being the smallest and Ca the largest cation that can be accommodated. The bond-valence sums of 1.73 v.u. around Mg in pyrope and 2.51 around Ca in grossular indicate that the cavity containing the divalent cation has a limited ability to accommodate cations of different sizes, being too large for Mg and too small for Ca.

Garnet is composed of $SiO_4$ tetrahedra sharing corners with $AlO_6$ octahedra to form a three-dimensional network in which the divalent $M$ cations, Mg or Ca, occupy eight-coordinate cavities. The cubic crystal structure has only four degrees of freedom, the lattice parameter and the three coordinates of the O atom, and these must be chosen to match the rigid geometry of the $SiO_4$ group and the expected lengths of the Si—O, Al—O and the two crystallographically distinct $M$—O bonds. The structure is therefore overdetermined, which accounts for its inability to accommodate Mg and Ca without strain. Garnet is a classic example of a constrained structure.

The framework bonds Si—O and Al—O behave as predicted by theory, but with the compressed Ca atom causing a slightly larger expansion in grossular. However, the Mg—O and Ca—O bonds show anomalously low values of both $dR/dT$ and $dU(+)/dT$ (see the filled circles in Fig. 5). These anomalies are easily understood when it is realized that the size of the cavity is entirely determined by the framework, so that cavity and framework must expand at the same rate. The exception to the above is the weaker of the two Mg—O bonds, which has much larger values of $dR/dT$ and $dU(+)/dT$ than would be expected from the properties of the framework. This is a consequence of Mg being too small for its cavity and being free to move along the direction of the weak Mg—O bonds. The distortion theorem predicts that Mg should be displaced from the centre of the cavity, but because of the high symmetry, this displacement will occur randomly, accounting for the soft behaviour of Mg in this direction. A similar conclusion was reached by Pilati, Demartin & Gramaccioli (1996) in their lattice dynamical study of garnets including grossular and pyrope. They provide an extensive bibliography of previous work on this system.

4.3.6. *$BaSO_4$ (h).* The structure of the $\gamma$ phase was studied by Sawada & Takeuchi (1990) between 298 and 1308 K. Structures determined above 1200 K were excluded from the study as they show anomalies associated with the transformation to the $\alpha$ phase at 1363 K.

Ba is shown as eight-coordinate, but there are two longer bonds that have not been included in the calculations, hence the theoretical bond valences of the Ba—O1 and Ba—O2 bonds are unrealistically large with consequent predictions of $dR/dT$ and $dU/dT$ that are much too low. Inclusion of the extra bonds just biases the predictions in the opposite direction. The lattice strains result in the observed structure lying between these two extremes. Because Ba is a heavy atom, the force constants calculated using (10) are overestimated, the theoretical values of $dR/dT$ and $dU/dT$ underestimated and the correlation coefficient $f$ overestimated.

4.3.7. *$MgGeO_3$ clinopyroxene (i).* Yamanaka, Hirano & Takeuchi (1985) determined this structure between room temperature and 1093 K just below the transformation to orthopyroxene. To avoid problems close to the transition, the highest temperature determination was not used.

The structure consists of chains of corner-sharing $GeO_3$ groups which run parallel to double chains of edge-sharing $MgO_6$ octahedra along the $c$ axis. Expansion of the crystal in the chain direction is determined by the small expansion of the strongly bonded $GeO_3$ chains. This in turn is responsible for the small expansion of the stronger Mg1—O1 and the Mg2—O2 bonds, which are the bonds most constrained by the $c$ axis expansion. The expansion of the other Mg—O bonds compensates by being slightly larger than expected as a consequence of the redistribution of the valence around Mg. The extensive study of thermal expansion of ternary pyroxenes by Cameron, Sueno, Prewitt & Papike (1973) discusses these constraints in some detail.

4.3.8. *$KLiSO_4$ (j).* Schulz, Zucker & Frech (1985) have determined this structure between room temperature and 568 K. It consists of a relatively flexible framework of corner-shared $LiO_4$ and $SO_4$ tetrahedra with nine-coordinated K filling the cavities within the framework.

Since Li has very few electrons, its position cannot be accurately determined using X-ray diffraction, making the observed lengths of the Li—O bonds unreliable, and because $R$, $dR/dT$ and $dU/dT$ are extremely sensitive to small variations in bond valence for weak bonds, the theoretical calculations of these quantities for the K—O bonds also unreliable. The structure was included because it is the only one, apart from $LiIO_3$, that contains bonds with valences less than 0.2 v.u. The contraction of the S—O bonds on heating can be ascribed to the librational motion of the rigid $SO_4$ groups, although when Schulz *et al.* (1985) corrected the bond lengths for libration, a significant contraction remained for S—O1, an effect they attribute to anharmonic librations that are not included in the normal riding model correction (Busing & Levy, 1964). Given the uncertainties inherent in both the theoretical and experimental values for this compound, the agreement is satisfactory.

4.3.9. *$Al_2SiO_5$ (k, l).* This compound is known in three polymorphs, of which the structures of the andalusite ($k$) and sillimanite ($l$) phases have been determined between room temperature and 1273 K by Winter & Ghose (1979). These structures are composed of rutile-like chains of $Al1O_6$ octahedra and corner-sharing double chains composed of $SiO_4$ and $Al_2O_4$ tetrahedra, both running parallel to the $c$ axis.

The observed values of $dU(+)/dT$ and $dR/dT$ are close to the expected values, except around the rutile-

like atom Al1 in andalusite. Its expansion along the $c$ axis (involving the bonds Al1—O1 and Al1—O3) is restricted by the smaller expansion of the more strongly bonded tetrahedral chain, since both chains must expand at the same rate. Consequently, the major expansion around Al1 occurs in the Al1—O4 bonds that are arranged perpendicular to **c**. In andalusite this bond is already excessively stretched (the bond valence is much lower than expected) and consequently it has a large value of $dU(+)/dT$ and a correspondingly large thermal expansion.

## 5. Conclusions

The present work provides a theoretical relation between thermal expansion and bond valence which is confirmed by observation (Fig. 5), but which differs significantly from the empirical relations (1) and (2) previously proposed by Megaw (1939) and Hazen & Prewitt (1977).

The thermal expansion of chemical bonds is a consequence of the anharmonic nature of the interatomic potential which is driven to a large extent by the exponential drop-off in the repulsion between atomic cores. It is this repulsive potential which determines how close two atoms can approach and which is reflected in the form of (3) and hence in the distortion theorem. It is therefore not surprising that application of the distortion theorem gives an essentially correct prediction of the thermal expansion of bonds according to the theory developed in §2.

Despite the many approximations that have been made in deriving the theory, the predictions of $dR/dT$ are sufficiently accurate to reveal the influence of spatial constraints and bond strains. Fig. 4 shows that a theory which uses only three fitted parameters, none of which has been fitted to any of the thermal properties of the bond, gives an accurate prediction of the average thermal expansion of bonds around individual cations. The scatter of points representing the thermal expansion of individual bonds shown in Fig. 5 indicates clearly that such expansion is not in general isotropic, but the anisotropies have been shown to arise from strains and constraints in the structure. Bonds that are stretched are weaker, have larger amplitudes of thermal motion and larger thermal expansion than those that are compressed (*e.g.* the bonds around Ni2 in $Ni_2SiO_4$). In constrained structures bonds are prevented from expanding along the constrained directions (*e.g.* Mg1—O1 and Mg2—O2 in pyroxene and Mg—O and Ca—O in garnet). Where possible, the expansion perpendicular to the constrained direction is larger than predicted so that the average expansion is close to the theoretical value. Such an effect represents a redistribution of the valence among the different bonds as the temperature changes.

The theory also makes predictions about the rate of increase in the amplitude of the thermal vibration of the bonds, $dU/dT$, which agrees well with the observed changes in the thermal vibrations of the atoms that form the bond. A comparison of the theoretical and observed values allows one to calculate the extent to which the motions of the terminal atoms are correlated (Fig. 6). Such correlations are significant for all but the weakest bonds, increasing with valence according to an exponential law with a constant of 0.5 v.u., until the bonds become essentially rigid at valences above 1.0 v.u.

IDB would like to thank the Natural Science and Engineering Research Council of Canada for an operating grant that made this work possible and AM would like to thank the Theme School of New Materials at McMaster University for financial assistance.

### References

Amos, D. W. & Flewett, G. W. (1974). *Spectrochim. Acta A*, **30**, 453–461.
Armbruster, A. (1976). *J. Phys. Chem. Solids*, **37**, 321–327.
Bergerhoff, G., Sievers, R., Hundt, R. & Brown, I. D. (1983). *J. Chem. Inf. Comput. Sci.* **23**, 66–69.
Brese, N. & O'Keeffe, M. (1991). *Acta Cryst.* B**47**, 192–197.
Brown, I. D. (1992). *Acta Cryst.* B**48**, 553–572.
Brown, I. D. & Altermatt, D. (1985). *Acta Cryst.* B**41**, 244–247.
Busing, W. R. & Levy, H. A. (1964). *Acta Cryst.* **17**, 142–146.
Cameron, M., Sueno, S., Prewitt, C. T. & Papike, J. J. (1973). *Am. Mineral.* **58**, 594–618.
Coquet, E., Crettez, J. M., Pannetier, J., Bouillot, J. & Damien, J. C. (1983). *Acta Cryst.* B**39**, 408–413.
Deverajan, V. & Shurvell, H. F. (1977). *Can. J. Chem.* **55**, 2559–2563.
Galanov, E. K. & Brodskii, I. A. (1969). *Sov. Phys. Solid State*, **10**, 2678–2682.
Hazen, R. M. & Prewitt, C. T. (1977). *Am. Mineral.* **62**, 309–315.
Hirschfeld, F. E. (1976). *Acta Cryst.* A**32**, 239–244.
Husson, E., Repelin, Y., Dao, N. Q. & Brusset, H. (1977). *J. Chem. Phys.* **67**, 1157–1163.
Ishiguro, T., Ishizawa, N., Mizutani, N. & Kato, M. (1982). *J. Solid State Chem.* **41**, 132–137.
Jones, L. H., Swanson, B. I. & Kubas, G. J. (1974). *J. Chem. Phys.* **61**, 4650–4655.
Kodama, N., Tanaka, K., Utsunomiya, T., Hoshino, Y., Marumo, F., Ishizawa, N. & Kato, M. (1984). *Solid State Ion.* **14**, 17–24.
Lager, G. A. & Meagher, E. P. (1978). *Am. Mineral.* **63**, 365–377.
Meagher, E. P. (1975). *Am. Mineral.* **60**, 218–228.
Megaw, H. D. (1939). *Z. Kristallogr.* **100**, 58–76.
Müller, A. & Krebs, B. (1967). *J. Mol. Spectrosc.* **21**, 180–197.
Pilati, T., Demartin, F. & Gramaccioli, C. M. (1996). *Acta Cryst.* B**52**, 239–250.
Plihal, M. & Schaak, G. (1970). *Phys. Status Solidi*, **42**, 485–496.
Sawada, H. & Takeuchi, Y. (1990). *Z. Kristallogr.* **191**, 161–171.
Schomaker, V. & Trueblood, K. N. (1968). *Acta Cryst.* B**24**, 63–76.

Schulz, H., Zucker, U. & Frech, R. (1985). *Acta Cryst.* B**41**, 21–26.
Smyth, J. R. (1975). *Am. Mineral.* **60**, 1092–1097.
Svensson, C., Albertson, J., Liminga, R., Kvick, A. & Abrahams, S. C. (1983). *J. Chem. Phys.* **78**, 7343–7351.
Willett, R. D., LaBonville, P. & Ferraro, J. R. (1975). *J. Chem. Phys.* **63**, 1474–1477.
Winter, J. K. & Ghose, S. (1979). *Am. Mineral.* **64**, 573–586.
Yamanaka, T., Hirano, M. & Takeuchi, Y. (1985). *Am. Mineral.* **70**, 365–371.